Surface degradation process affected by heterogeneity in nano-titanium dioxide filled acrylic urethane coatings under accelerated UV exposure

Yongyan Pang [a, b, *], Stephanie S. Watson [b], Li-Piin Sung [b]

[a] *Polymers and Composites Division, Ningbo Institute of Materials Technology & Engineering, Chinese Academy of Sciences, Ningbo, Zhejiang Province 315201, China*

[b] *Polymeric Materials Group, Engineering Laboratory, National Institute of Standards and Technology, Gaithersburg, MD 20899, United States*

ABSTRACT

The objective of this study was to investigate the effect of nanoparticle dispersion on surface morphological changes and degradation process in polymeric coatings during exposure to ultraviolet (UV) radiation. Three types of nano-titanium dioxide (nano-TiO_2) were selected and dispersed into acrylic urethane (AU) coating to generate degrees of nanoparticle dispersion states. Two accelerated exposure conditions: wet (30 °C and 75% relative humidity (RH)) and dry (30 °C and 0% RH), were selected. Attenuated total reflectance-Fourier transform infrared spectroscopy (ATR-FTIR) was used to monitor surface chemical degradation. Laser scanning confocal microscopy (LSCM) was used to characterize nanoparticle dispersion and surface/subsurface morphological changes in the AU coatings during UV exposure. For a given nanoparticle, similar surface morphological changes of the coatings indicated the similar degradation processes under the wet and dry conditions, but the degradation was faster under the wet condition. Surface morphological changes were closely related to the nanoparticle dispersion in three coatings, and the heterogeneity in nanoparticle dispersion significantly affects the degradation process and dominates the degradation patterns.

1. Introduction

In recent years, nanoparticles have been added to polymer matrices to enhance their mechanical and appearance properties in automotive, aerospace, infrastructure, and manufacturing applications [1—3]. It is well-known that the surface properties of polymeric systems differ greatly from their bulk properties and that the surface is the first target in any degradation process initiated by ultraviolet (UV) radiation, mechanical stress (via scratch and abrasion), temperature, and/or moisture [4,5]. Surface damage causes changes in optical and morphological properties, such as gloss loss, yellowing, chalking and cracking, which significantly affect the long-term performance of these complex materials. The purpose of this study was to investigate the effect of surface and subsurface heterogeneity in nano-TiO_2 filled polymeric coatings on the surface degradation process under the exposure of UV radiation and moisture. A nano-titanium dioxide (TiO_2) filled acrylic urethane (AU) coating was chosen due to its wide use. Three types of commercial nano-TiO_2 were selected for this study to generate different degrees of filler dispersion and microstructural heterogeneity.

TiO_2 is a photoreactive material, with level of photoreactivity dependent on the crystal type, size, and surface treatment. Preferably, a series of nano-TiO_2 particles with the same size, crystal form and photoreactivity, but different surface functionality would be the best to generate different dispersion state. However, it is difficult to obtain commercial nano-TiO_2 particles of similar crystal size, form and photoreactivity. In this study, three types of nano-TiO_2 with similar crystal size but varying levels of photoreactivity were selected: an anatase form, a rutile form, and a mixed crystal form of anatase and rutile. According to the reported studies [6—12], an anatase form is generally more photo-active than a rutile form, and a mixed crystal form of them possesses a higher photoreactivity than an anatase form due to a possible synergetic effect. In this study, it is highly expected that the varying levels of photoreactivity of the nanoparticles may have varying effects on the photodegradation of the coatings. And with photodegradation

---

* Corresponding author. Polymers and Composites Division, Ningbo Institute of Materials Technology & Engineering, Chinese Academy of Sciences, Ningbo, Zhejiang Province 315201, China. Tel.: +86 574 87616292; fax: +86 574 86685186.

E-mail address: yongyan.pang@nimte.ac.cn (Y. Pang).

progressing, the dispersion effect of nanoparticles on polymer degradation process could be displayed.

Some studies have been carried out to investigate the effect of TiO_2 on the photodegradation of polymeric composites [13–17]. Clerici et al. [13] investigated the effect of pigmentary TiO_2 dispersion on the durability of epoxy coatings. Dispersant was employed to prepare "well dispersed" and "poorly dispersed" specimens. They found that difference in dispersion state played a significant role in polymer degradation. Wang et al. [14] investigated the effect of TiO_2 pigment type in terms of surface treatment, particle size and dispersion on the photodegradation of filled coatings. In their study, nanosize TiO_2 with high photoreactivity and micron size TiO_2 with low photoreactivity were used. It was found that both particle dispersion and photoreactivity had a significant effect on the degradation of the polymeric coatings. However, in their study, two exposure conditions selected were an ambient, dry condition [25 °C and 0% relative humidity (RH)] and a high temperature, wet condition (55 °C and 75% RH), where the effect of humidity and temperature on photodegradation were not separated. Moreover, nanosize and micron size TiO_2 were used, instead of only a series of nanosize or micro size TiO_2. Based on the previous study [17], compared to micro size TiO_2, the nanosize TiO_2 shows higher photoreactivity due to its much larger surface area. Also, the dispersion of nanosize TiO_2 in coatings is expected to be different compared to that of its micron size counterpart. In this study, a series of nano-TiO_2 were selected to study the effect of nanoparticle dispersion on the degradation process of polymeric coatings, which has not thoroughly understood so far.

The objective of the present work was to study the effect of heterogeneity in nano-TiO_2 dispersion on the UV-initiated surface degradation process in three nano-TiO_2 filled AU coatings with moisture. Two accelerated exposure experiments: wet (30 °C and 75% relative humidity (RH)) and dry (30 °C and 0% RH), were carried out using the NIST SPHERE (Simulated Photodegradation via High Energy Radiant Exposure) [18,19]. Laser scanning confocal microscopy (LSCM) was used to characterize the nano-TiO_2 dispersion and monitor the surface and subsurface morphological changes in the polymeric coatings during UV exposure. Attenuated total reflectance-Fourier transform infrared spectroscopy (ATR-FTIR) was used to monitor surface chemical degradation. To quantify the degradation rate, the changes in the peak intensity of some IR bands as a function of UV exposure time were calculated. It was found that nanoparticle dispersion dominated the surface morphological changes during UV radiation and significantly affected the degradation process of the filled coatings.

2. Experimental

2.1. Materials and sample preparation

[1] The three commercial nano-TiO_2 used in this study are designated as P_A, P_B, and P_C. The crystal type, average crystal size, surface treatment, and relative photostability [11] of these materials are listed in Table 1.

The preparation of nano-TiO_2/AU films is as follows: (1) Nanoparticles were added slowly into acrylic resin (Joncryl 588, BASF) and stirred using a high speed mechanical mixer (Dispermat − BYK Gardner) at 52.4 rad/s for 10 min; followed by continuous mixing at 366.5 rad/s for 30 min; (2) isocyanate (Desmdur N3200, Bayer) was added to the mixture at a 65/35 acrylic/isocyanate mass ratio and

Table 1

Nano-TiO_2 particles were labeled as P_A, P_B, and P_C. Crystal type, average crystal size, and surface treatment were provided by manufacturers. The relative photostability was measured by a spin trap method using electric paramagnetic resonance (EPR) measurements [11]. A higher value represented a higher photostability and thereby a lower photoreactivity level.

Label	P_A	P_B	P_C
Crystal	anatase (70%) rutile (30%)	rutile	anatase
Average crystal size (nm)	20	30–50	35
Surface treatment	none	Al(OH)$_3$	organic
Relative photostability	9%	97.62%	74.85%

mixed at 366.5 rad/s for an additional 10 min; (3) the mixture was degassed for 2 h in a vacuum oven; (4) the mixture was applied to release paper using a drawdown technique; (5) film samples were cured at room temperature overnight, and then post-cured at 130 °C for 30 min. The thickness of dry film was approximately 110 μm measured by micrometer. The same loading of particle volume concentration (PVC) was kept constant of 5% for all samples.

2.2. UV exposure experiments

Film specimens were mounted in a sample holder and exposed using an advanced accelerated UV weathering chamber, the NIST SPHERE [18,19]. The SPHERE generates high intensity UV radiation and allows accelerated photodegradation of exposed specimens to be carried out. The SPHERE is equipped with environmental chambers in which temperature, humidity, and UV spectral irradiance can be individually controlled. In this study, two exposure conditions were selected: a wet condition (30 °C and 75% RH) and a dry condition (30 °C and 0% RH). Surface chemical and morphological changes in the nano-TiO_2 filled coatings were characterized at sequential intervals using ATR-FTIR and LSCM.

2.3. Attenuated total reflectance-Fourier transform infrared spectroscopy (ATR-FTIR)

ATR-FTIR analysis was performed using a Nexus 670 (Thermo Nicolet) with an MCT detector and an ATR accessory with a diamond crystal (Durascope). Each specimen was sampled at three different locations, and 128 spectra with 4 cm^{-1} resolution were collected at each location. A background scan was collected before each new sample. A custom software package was used to normalize, baseline correct and analyze the data. Note that the ATR results are strongly affected by the surface roughness of the overall contact area.

2.4. Laser scanning confocal microscopy (LSCM)

A Zeiss model LSM510 reflection laser scanning confocal microscope (LSCM) was employed to characterize nanoparticle dispersion and the surface/subsurface morphology in AU coatings. A detailed description of LSCM can be found in the literature [20,21]. The laser wavelength was 543 nm and images were taken at a magnification of 150×, with optical slice (z-step) of 0.1 μm for AU coatings containing P_A or P_B, and 0.2 μm containing P_C. To eliminate the strong reflection from polymer surface, an oil lens with a magnification of 100× and a numerical aperture of 1.30 was used to image the particle dispersion inside the coatings. LSCM graphs shown here were two dimensional (2D) projection images in xy plane and in xz plane, and a single frame depth − profile image in xy plane at a z − depth of 3.0 μm 2D (xy) projection image in the xy plane (512 pixel × 512 pixel) was formed by summing the

stacks of the image in the *z* direction of the coatings, while the 2D (xz) side projection image was projected in lateral xz plane in the *y* direction. The depth − profile was a single layer selected from the stack of the image, which displayed the microstructure and nanoparticle agglomerate distribution in the subsurface of polymeric coatings. Pixel intensity level represented the total amount of backscattered light. Lighter areas represented regions that scatter more light than darker areas.

The morphology change of AU coatings under UV exposure was also characterized using LSCM equipped with a custom-designed stage to reproducibly image the same location in the specimen each time. In this way, morphology evolution at the same location can be monitored as a function of exposure time. The root mean square (RMS) [14] surface roughness, R_q, was calculated to quantify the morphology changes in surface and subsurface of coatings during the UV exposure. Eqs. (1) and (2) were used to calculate R_q from the 3D topographical images:

$$R_q = \sqrt{\frac{1}{N_x \cdot N_y} \cdot \sum_{i=1}^{N_x} \cdot \sum_{j=1}^{N_y} \cdot [z(x_i, y_i) - R_c]^2} \tag{1}$$

$$R_c = \frac{1}{N_x \cdot N_y} \cdot \sum_{i=1}^{N_x} \cdot \sum_{j=1}^{N_y} \cdot z(x_i, y_i) \tag{2}$$

where N_x and N_y are the number of pixels in the x- or y-direction. An automatic plane fit along with a numerical filter (3 × 3) was used in this case. The R_q values presented here were the averaged RMS surface roughness values obtained at 4 measurements from each scanned area of 56.1 μm × 56.1 μm. The error bar represented the standard deviation from a mean value.

3. Results and discussion

3.1. Nanoparticle dispersion and heterogeneous microstructure

Fig. 1 displays 2D (xy and xz) LSCM projections and depth-profile images at 3.0 μm below polymer surface for all AU nano-TiO₂ coatings. Since the refractive index of TiO_2 particles is higher than that of the polymer matrix, the bright spots represent TiO_2 nanoparticles on or near the surface while dark regions are associated with the polymer matrix. The backscattered intensity of a particle agglomerate depends strongly on the size of agglomerate ($I \propto size^6$) and the packing of the nanoparticles in the agglomerate. Larger agglomerates appear much brighter than the smaller ones.

The 2D (xy) projection images (Fig. 1a) of AU − P_A and AU − P_B showed small bright spots uniformly distributed. However, there were very few bright spots on the surface of AU − P_C. This implies that most of P_C TiO_2 particles were buried deep into the polymer matrix. This observation is confirmed by the 2D (xz) side projection images (Fig. 1b). For AU − P_A, the particles were distributed uniformly and tightly packed near the surface. However, for AU-P_C, the particle agglomerates were loosely packed and the Z-depth was larger. Z-depth, defined as the total scanning or laser penetration depth in the *z* direction (shown in Fig. 1b) was around 8 μm for AU − P_A, 12 μm for AU − P_B, and 20 μm for AU − P_C. To more closely investigate the nanoparticle dispersion (particle shape and size) inside the film, depth profiling was carried out at 3.0 μm below the polymer surface, as shown in Fig. 1c. P_A agglomerates were smaller than 500 nm and uniformly distributed in the AU coating, most of the P_C agglomerates were spherical in shape and had diameters as large as 10 μm, and P_B agglomerates were elliptical and randomly distributed throughout the AU coating with sizes intermediate between P_A and P_C agglomerates.
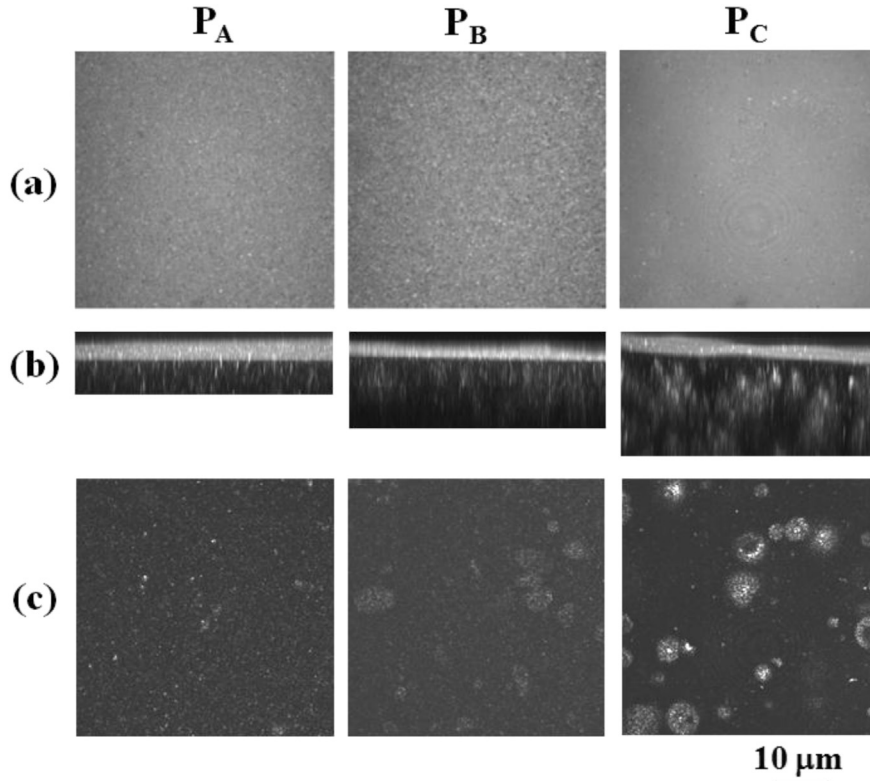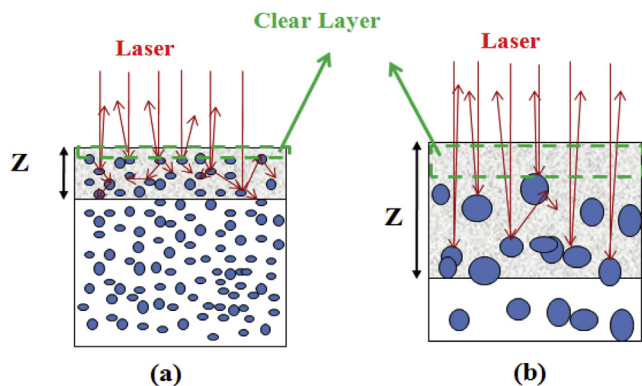

Fig. 1. LSCM images of AU coatings containing P_A, P_B, and P_C: (a) 2D (xy), (b) 2D (xz), and (c) depth-profile (xy) at 3 μm below polymer surface. The scale bar was 10 μm.

Fig. 2. Illustration of laser penetration in coatings (a) with small and densely packed particles, and (b) with large and a fewer particles. Z indicated laser penetration depth. The green boxes showed the clear layer regions in both cases. (For interpretation of the references to color in this figure legend, the reader is referred to the web version of this article.)

As mentioned above, the Z depth is larger in $AU - P_C$ than in $AU - P_A$ (as shown in Fig. 1b), and the result can be illustrated in Fig. 2, which is more comprehensible. Fig. 2a illustrates a smaller penetration depth in coatings containing densely packed, small particles (similar to $AU - P_A$), while Fig. 2b shows a larger penetration depth with fewer, larger particles (similar to $AU - P_C$). Because the smaller P_A agglomerates were uniformly distributed and densely packed near the surface layers, they scattered most of the incident laser light near the surface, preventing the laser from penetrating deeper; consequently, Z depth was smaller for coatings formulated with P_A. In comparison, fewer and larger P_C agglomerates were buried deep inside the films. Less light was scattered near the polymer surface, while instead, it penetrated deeper and was reflected back by larger particle agglomerates, and thereby, Z depth was larger.

It was observed that most of the large P_C particle agglomerates sank to the bottom of the wet coating after the drawdown

application and were buried deep inside the cured film. This resulted in a much thicker clear layer for coatings formulated with P_C than with P_A and P_B (as illustrated in Fig. 2b). A clear layer was defined as a layer of unpigmented (or pigment-poor) medium formed at the surface of a pigmented coating [22]. As the P_A or P_B particle agglomerates were distributed densely on the surface and subsurface layers, the clear layer was quite thin; in comparison, the clear layer was much thicker for coatings formulated with P_C. Clerici et al. [13] also observed the clear layer in their study, and a thinner clear layer was formed in the "well dispersed" specimen, while a thicker one in the "poorly dispersed" specimen.

To achieve a better dispersion measurement, a high numerical aperture oil lens with index match oils was used to eliminate the light scattered from polymer surface. Fig. 3a shows 2D LSCM images of AU coatings containing P_A, P_B, and P_C, respectively, obtained using an oil lens ($100\times/1.30$). Clearly, the distribution of P_A in AU was more uniform than that of P_B and P_C, and the agglomerate sizes of P_C were larger than those of P_A and P_B. To quantify the size distribution of agglomerates, the freeware *ImageJ* [23] was used to process image threshold and analyze agglomerate size. Fig. 3b displays the corresponding threshold images of the 2D LSCM images in Fig. 3a. The size distributions of P_A, P_B, P_C agglomerates are listed in Table 2. Noticeably, the majority of agglomerate size was $\leq 0.5\ \mu m$ (at resolution limit at this magnification) in all three cases. However, P_A agglomerates had a narrower size distribution than that of P_B and P_C agglomerates. The degree of dispersion, DoD, (or polydispersity index) can be calculated as follows:

$$DoD = \frac{d_w}{d_n} \qquad (3)$$

where $d_n = \left(\sum_{i=1}^{N} n_i \cdot d_i\right)/\left(\sum_{i=1}^{N} n_i\right)$ and $d_w = \left(\sum_{i=1}^{N} n_i \cdot d_i^2\right)/\left(\sum_{i=1}^{N} n_i \cdot d_i\right)$ are the number and weight averaged agglomerate sizes, respectively. The values of d_n, d_w and DoD for each of the AU systems are listed in Table 3. P_A had the lowest DoD of 1.12, followed by P_B with a DoD of 1.27, and P_C with the highest of 1.98. As a lower DoD corresponds to better dispersion, the best AU nanoparticle dispersion
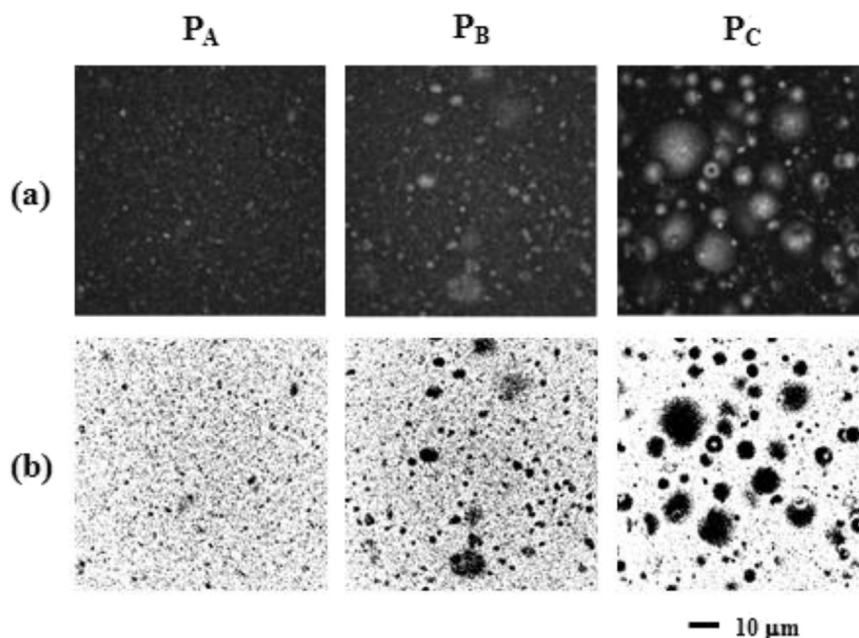
Fig. 3. (a) 2D LSCM images obtained using an oil lens ($100\times/1.30$) of AU coatings containing P_A, P_B, and P_C; (b) the corresponding threshold images for agglomerate sizing. The scale bar was 10 μm. Size of each image was 84.2 μm × 84.2 μm.

Table 2
The size distribution of nano-TiO$_2$ (P$_A$, P$_B$, P$_C$) agglomerates in the AU coatings obtained from threshold images in Fig. 3b.

Agglomerate size, d (μm)	P$_A$	P$_B$	P$_C$
$d \leq 0.5$	7331	7546	2971
$0.5 < d \leq 1$	893	858	164
$1 < d \leq 1.5$	112	131	28
$1.5 < d \leq 2$	15	47	15
$2 < d \leq 2.5$	3	24	13
$2.5 < d \leq 3$	2	5	6
$3 < d \leq 5$		10	18
$5 < d \leq 10$		5	13
>10			1

Table 3
The number averaged size (d_n), weight averaged size (d_w), and degree of dispersion (DoD) for nano-TiO$_2$ (P$_A$, P$_B$, P$_C$) agglomerates in the AU coatings. The definitions of these parameters were described in the Eq. (3). The estimated uncertainties in d_n, d_w and DOD were approximately 5%.

Label	P$_A$	P$_B$	P$_C$
d_n	0.57	0.59	0.60
d_w	0.64	0.75	1.19
DoD = (d_w/d_n)	1.12	1.27	1.98

among the three types of nanoparticles was found in the AU − P$_A$ coating, while the worst was in the AU − P$_C$ coating. Visual heterogeneity in terms of particle size and distribution was also the most obvious in the AU − P$_C$ coating. It is claimed that the nanoparticles used in this study were in the states as they were commercially supplied, without any further surface modification to adjust the dispersion. Thereby, the various nanoparticle dispersion states presented in this study were what they were formed.

The confocal image obtained using an oil lens is consistent with that obtained using regular lens. However, the oil lens method is a contact measurement and provides no information on surface morphology. For the purpose of monitoring surface/subsurface degradation, the LSCM images presented later in this paper were generated using 150×/0.95 regular lens. As discussed above, different degrees of nanoparticle dispersion were obtained with the different type of nano-TiO$_2$. The heterogeneity in microstructure and dispersion was expected to impact the surface degradation of polymeric coatings under UV exposure. Thereby, the remainder of the paper will focus on the effect of nanoparticle dispersion on morphological changes in AU coatings under wet and dry conditions with UV exposure.
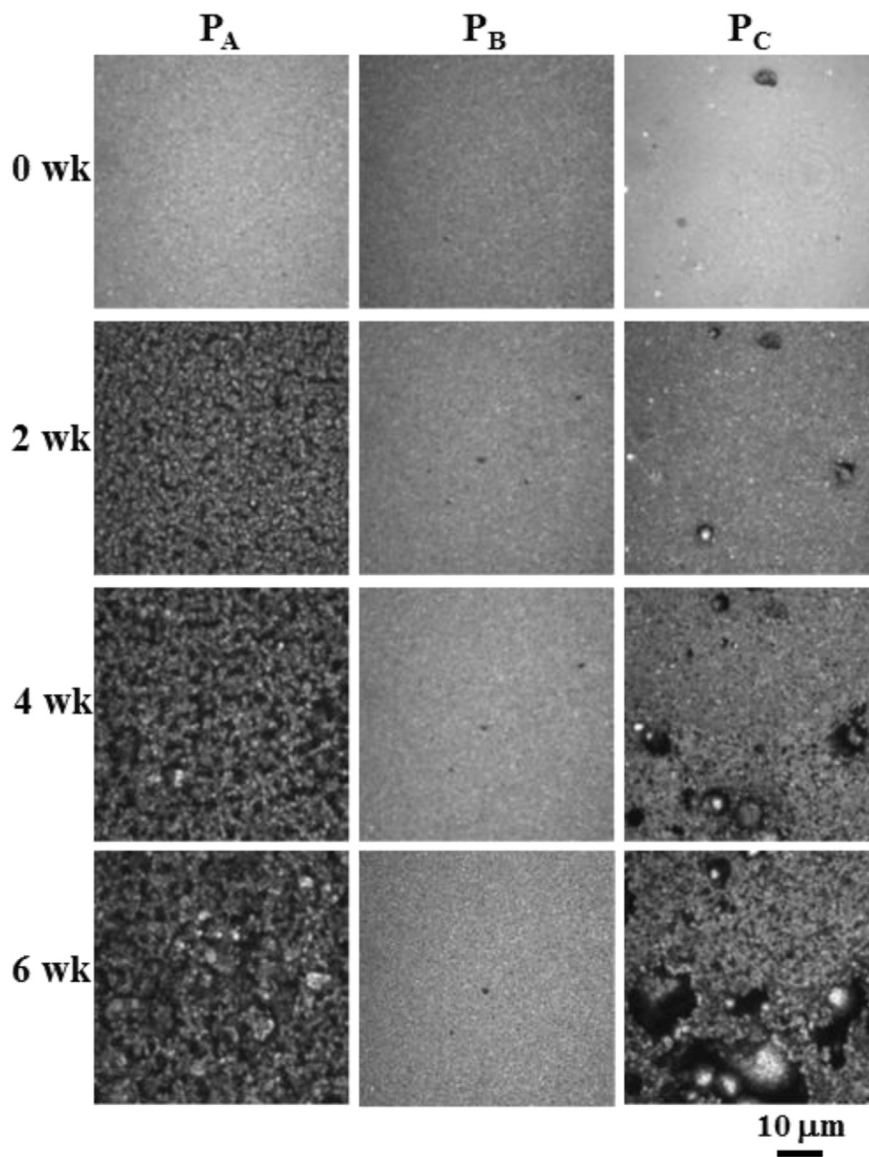
3.2. UV exposure under wet condition

Fig. 4 shows the surface morphology changes initiated by UV exposure under the wet condition for the three nano-TiO$_2$ filled AU coatings. The images were obtained at the same location on each sample. For the AU − P$_A$ coating, a network-like degradation pattern was observed on the surface around week 2. It appeared that the polymer degraded around the uniformly distributed P$_A$ agglomerates, and then the eroded areas connected, forming a network-like pattern. Gradually, the network-like pattern became coarser as the degradation progressed. And the darker regions, corresponding to the eroded sections, became larger and larger. In comparison, the surface morphology of the unfilled AU coating (not shown here) exhibited no significant changes after a 6 − week period of UV exposure, and no distinguishable surface features were formed. This result implies that the incorporation of P$_A$ nanoparticles in AU coatings affected the surface morphology change during UV exposure. However, for the AU − P$_B$ coating, no significant

morphology changes were observed during the 6 − week UV exposure. For the AU − P$_C$ coating, uniform erosion of the clear layer was the first step of degradation on polymer surface, and then some degradation features appeared. The size of these features increased and some of them merged and increased in size after week 4. It was observed that once after the clear layer was eroded and the nanoparticles appeared onto polymer surface, the polymer surface degradation was not a uniform process any more. The polymer degradation kept progressing in the polymer-rich regions (or the nanoparticle-poor regions), while severe degradation was found in the vicinity of large particle agglomerates originally buried deep inside the films. Thereby, after the nanoparticles appeared onto polymer surface, the polymer degradation process became quite inhomogeneous for AU − P$_C$ coating due to its ununiformed nanoparticle dispersion.

By comparison of the polymer degradation in Fig. 4, dramatic difference of surface morphological changes was observed between AU − P$_A$ (DoD = 1.12) and AU − P$_B$ (DoD = 1.17), which was much more obvious than that of the dispersion of the two samples. It is probably attributed to the higher photoreactivity of P$_A$. For photoreactive TiO$_2$, when it absorbs UV radiation, free electrons are promoted from the valence band to the conduction band, leaving positively charged holes in the valence band. Both the electrons and the holes are capable of participating in photooxidation and thereby accelerate degradation of polymeric materials [10,14]. It is shown in Table 1 that the photoreactivity of the three nanoparticles is ranked as $P_A >> P_C > P_B$. Consequently, photodegradation was faster for AU − P$_A$ relative to AU − P$_C$ and AU − P$_B$. A parallel experiment without UV radiation under wet condition (30 °C, 75% RH) was carried out on the coatings containing photoreactive fillers of P$_A$ and P$_C$ (not shown here). No significant surface morphological changes were observed up to 12 weeks. Similar result was also reported in our previous work carried out at NIST about EVA systems, and no visible chemical or morphological changes were observed for specimens exposed to condition without UV radiation [24]. It implies that UV radiation was the primary factor in initiating the polymer degradation, relative to photoreactivity of the nanoparticles and humidity. As prominent photodegradation was observed in AU coatings containing P$_A$ and P$_C$ rather than P$_B$, it indicates that the photocatalytic effect of the nanoparticles played a prodegradant role during the photodegradation of the polymers, consistent with the previous literature [25].

Other than the effect of photoreactivity, Fig. 4 also demonstrates the effect of the nanoparticle dispersion on the degradation of the AU coatings. As it was described earlier in this section, uniform network-like degradation patterns were observed for AU − P$_A$, while inhomogeneous degradation for AU − P$_C$, with severer degradation occurring surrounding particle agglomerates than in the bulk matrix without fillers. The different surface morphological changes were closely related to the dispersion of photoreactive nanoparticles in the polymeric coatings. It has already been discussed that the nanoparticle dispersion in AU − Pc coating was very poor, with big agglomerates and small ones distributing in the matrix. As the interfacial area around a big nanoparticle agglomerate was larger than a small one, the polymer degradation was thereby much more prominent. Consequently, the photodegradation for the AU − Pc coating was quite inhomogeneous. Moreover, the degradation of AU − Pc seemed slower for the first 4 weeks, and after the nanoparticles appeared on the polymer surface, its degradation seemed to have speeded up. It is believed that the thicker clear layer in AU − P$_C$ was the possible cause for the slower surface degradation before week 4 (Fig. 2b). The polymer photodegradation might not be accelerated by the photocatalytic effect of the nanoparticles until they were exposed onto surface by erosion of the clear layer. To summarize, nanoparticle dispersion

Fig. 4. 2D LSCM images of AU − P_A, AU − P_B, and AU − P_C at different exposure times under the wet condition. The scale bar was 10 μm. Each image size was 56.1 μm × 56.1 μm.

was a significant factor contributing to the different degradation patterns between AU − P_C and AU − P_A. AU − P_C system had the worst nanoparticle dispersion (DoD = 1.98), and provided with exposure to UV radiation, it definitely displayed prominent localized degradation around the large nanoparticle clusters, which was consistent with the reported study [14]. The result implies that the effect of nanoparticle dispersion plays a significant role in the degradation process.

3.3. UV exposure under dry condition

The morphology change of AU − P_A and AU − P_C during UV exposure under the dry condition is shown in Fig. 5. For both samples, the patterns of morphological changes under the dry condition appeared to be similar to those observed under the wet condition, but the degradation was much slower. For example, the localized degradation around large nanoparticle agglomerates in the AU − P_C coating became visible around week 12 under the dry condition, compared to week 4 under the wet condition. It implies that surface degradation was accelerated at higher humidity at a

certain temperature. Previous literatures have interpreted that under UV radiation, photoexcited TiO_2 would produce electrons and positive holes, which would react with water and oxygen (existing in the experimental conditions) to form OH•. The hydroxyl radical would attack polymeric materials, resulting in accelerated polymer photodegradation [17,26,27]. Other studies also reported that water could be absorbed in coatings [28], higher humidity accelerated photodegradation of polymer films [24,29] and that prolonged exposure to moisture promoted more severe degradation in polymer coatings [30]. In summary, the moisture/humidity plays a role in accelerating the photodegradation of polymer coatings containing high photoreactive nanoparticles under UV radiation.

3.4. Rate of UV degradation

One of the methods to quantify UV degradation rate is to measure chemical changes in the degraded polymers, e.g. using data obtained from ATR-FTIR measurements as a function of exposure time [21,31,32]. In this study, changes in two infrared (IR) bands
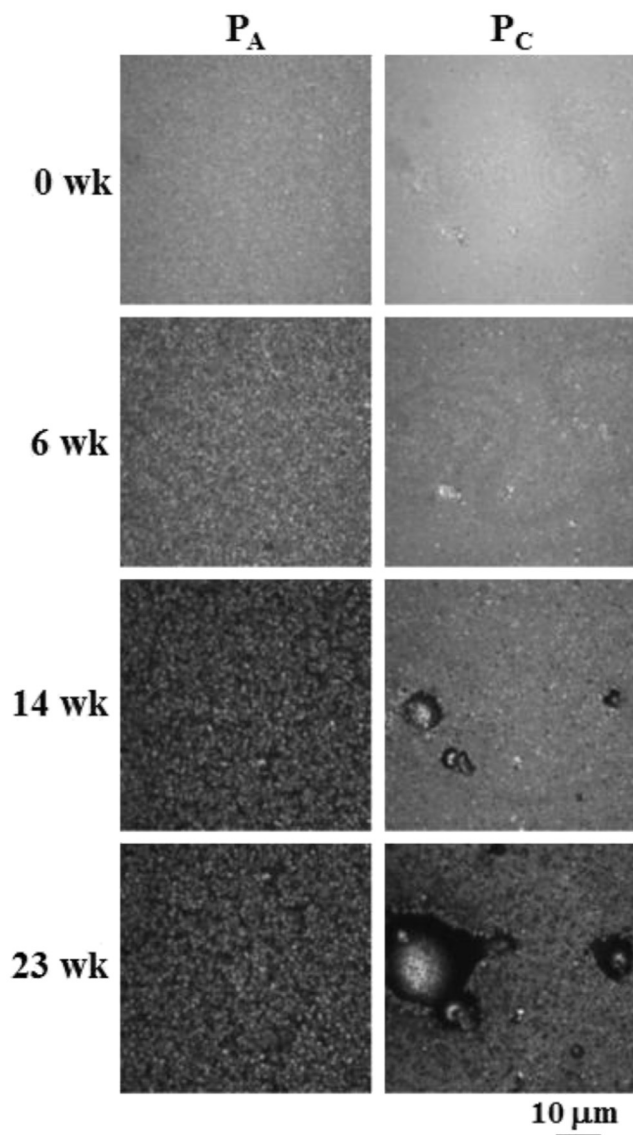
$$\text{Relative Change @ } 1724\,\text{cm}^{-1} = 100*\left(\frac{A_{t,1724\text{cm}^{-1}}}{A_{t,2933\text{cm}^{-1}}} - \frac{A_{0,1724\text{cm}^{-1}}}{A_{0,2933\text{cm}^{-1}}}\right)$$
(5)

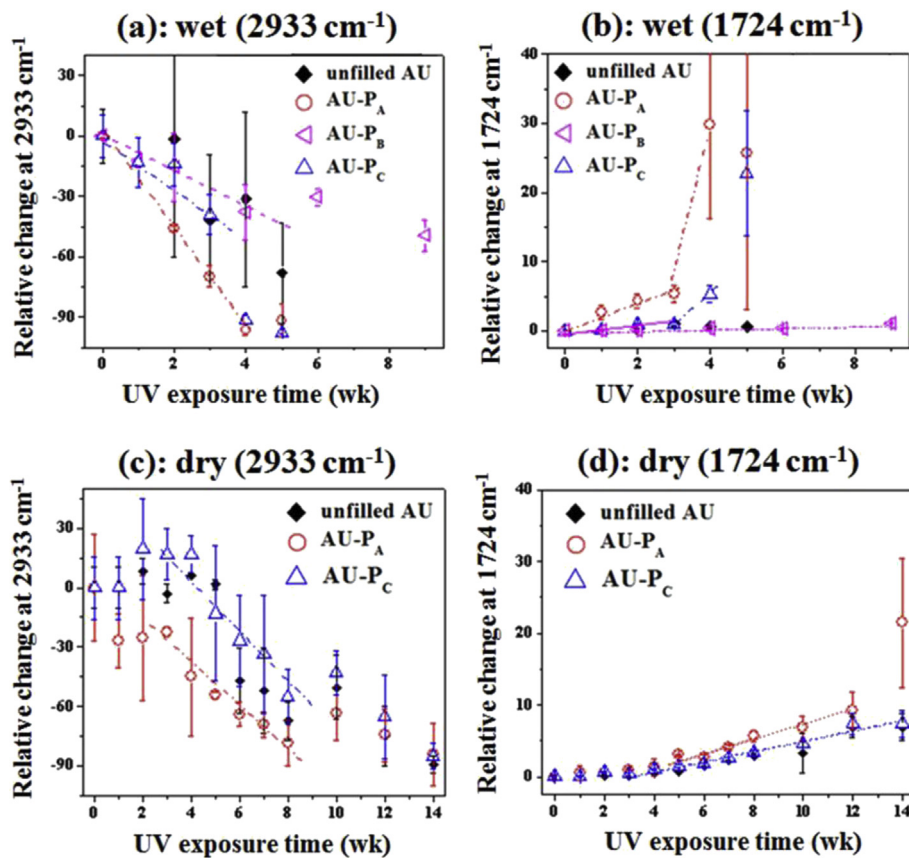where $A_{0,2933}$, $A_{t,2933}$, $A_{0,1724}$, and $A_{t,1724}$ are the IR absorbance values at 2933 cm^{-1} and 1724 cm^{-1} determined for each specimen at 0 and t weeks of UV exposure.

Fig. 6 displays the relative changes in the absorbance of IR bands at (6a) 2933 cm^{-1} and (6b) 1724 cm^{-1} under the wet condition, and (6c) 2933 cm^{-1} and (6d) 1724 cm^{-1} under the dry condition. The relative loss in intensity of 2933 cm^{-1} was larger than 80% for AU-P_A and AU-P_C systems at week 4 under the wet condition and larger than 60% at week 8 under the dry condition. It indicates that the mass loss was accelerated under the wet condition, consistent with the surface morphological changes. However, the uncertainty increased and the measurements became unreliable with long exposure times due to the severe increase in surface roughness. The relative intensity change for 1724 cm^{-1} was increased under both wet and dry conditions, and the increase was a little bit faster for the former than the latter condition at the early stage. In comparison, the change in the 1724 cm^{-1} band was surprising lower, with an increase around 20 %$-$30 % as compared to 80% loss in the relative changes observed in 2933 cm^{-1} band. It probably indicates that part of the polymers was oxidized and major part was degraded under UV exposure.

Overall, in terms of relative changes in IR absorbance bands, AU $-$ P_A had the largest degradation rate in the earlier stages of degradation, followed by AU $-$ P_C, AU $-$ P_B and unfilled AU, as illustrated in Fig. 6a and b. Note that the unfilled AU did degrade under UV exposure. However, as its degradation was probably a homogeneous reduction in thickness, no significant surface morphological changes were observed within the experimental range, which might be the same phenomenon as the degradation in the clear layer. A previous study [21] indicates that mass loss corresponding to the changes in the C$-$H stretch band at 2933 cm^{-1} is only correlated to the film thickness changes in the early stage of the degradation process, during which coating surfaces remain relatively smooth. When the surface pits or protuberances grow larger, the uncertainties in the IR data also increase. Therefore, ATR-FTIR results cannot truly reflect the surface chemical degradation for the samples undergone a long-term UV exposure. Non-contact IR techniques such as photoacoustic IR spectroscopy will be utilized for further studies.

3.5. Degradation process affected by nanoparticle dispersion

ATR-FTIR turns out to be only feasible to study the early-stage degradation process for nanoparticle filled coatings, while LSCM is usually applied to investigate the morphological changes during a long-term degradation process as the measurements are non-contact and non-invasive. LSCM images provide detailed information on surface degradation, and can be used to monitor the surface morphological changes and surface roughness during UV exposure. Fig. 7a displays the average RMS roughness values as a function of UV exposure time for the unfilled AU and three filled AU coatings under the wet condition. The unexposed (week 0) AU $-$ P_C coating showed the largest surface roughness value, followed by AU $-$ P_B, then AU $-$ P_A and finally unfilled AU, in the same sequence as the nanoparticle dispersion heterogeneity. During UV degradation, roughness of the unfilled AU and AU $-$ P_B coatings did not change significantly, as no noticeable surface features were formed in these two coatings. In comparison, for AU $-$ P_A, a sharp increase in RMS roughness was observed between week 1 and week 2, which was related to the network-like structure formation (Fig. 4, left column).

Fig. 5. 2D LSCM images of AU $-$ P_A and AU $-$ P_C at different exposure times under the dry condition. The scale bar was 10 μm. Each image size was 56.1 μm × 56.1 μm.

were monitored: the decrease in C$-$H stretch band (2933 cm^{-1}), attributed to mass loss of the polymer, and the increase of the carbonyl C$=$O stretch band (1724 cm^{-1}), attributed to oxidation of the polymer matrix. The relative change in the intensity of the C$-$H stretch band at exposure time t was normalized by the absorbance of the band at 2933 cm^{-1} in the unexposed specimen (at exposure time $t = 0$). Eq. (4) was used to calculate the relative change:

$$\text{Relative Change @ } 2933\,\text{cm}^{-1} = 100*\left(\frac{A_{t,2933\text{cm}^{-1}}}{A_{0,2933\text{cm}^{-1}}} - 1\right)$$
(4)

where $A_{0,2933}$ and $A_{t,2933}$ are the IR absorbance values at 2933 cm^{-1} for each specimen at 0 and t weeks of UV exposure. Formation of oxidation products was measured by the relative change in C$=$O stretch absorbance. The relative change in the 1724 cm^{-1} band was calculated by normalization to the IR absorbance at 2933 cm^{-1} and the difference from the ratio of the unexposed specimen as shown in Eq. (5):

Fig. 6. Relative changes in the absorbance of IR bands at (a) 2933 cm^{-1} and (b) 1724 cm^{-1} under the wet condition, and at (c) 2933 cm^{-1} and (d) 1724 cm^{-1} under the dry condition, respectively for AU coatings. The error bars represented one standard deviation. The dashed lines were the visual guides to show the trend in changes. The relative changes were calculated based on Eqs. (4) and (5) in the text.

For AU − P$_C$, little change in roughness was observed before week 2 due to the lack of topographical changes during the erosion of the clear layer. Roughness began to increase at around week 3, which arose from the appearance of localized degradation features (Fig. 4, right column). The degradation features grew much larger after week 5 for AU − P$_C$ coating, and the corresponding RMS roughness value increased sharply as well, eventually surpassing that of AU − P$_A$ coating.

As discussed previously, similar morphological changes were observed under the wet and dry conditions for AU coatings containing the same nanoparticle. Fig. 7b displays RMS data for AU − P$_A$ and AU − P$_C$ as a function of exposure time under both conditions. For better comparison, all curves were normalized to the initial roughness value of AU − P$_C$ under the wet condition (AU − P$_C$ − wet) at time zero. The roughness of AU − P$_A$ and AU − P$_C$ under the wet condition increased much faster compared to their counterparts under the dry condition. To understand the correlation between the surface roughness and nanoparticle dispersion in the degraded coatings, the degradation process can be divided into three stages, similar as dividing it into three regions reported in the literature studying the relation between film thickness changes and chemical changes during UV degradation [21]. For example, for AU − P$_A$ under the wet condition (indicated as dashed lines in Fig. 7a), no significant changes in roughness were observed in the first stage (before t_1): this is due to the erosion of the thin clear layer. In the second stage (between t_1 and t_2), roughness increased dramatically due to the development of a network-like structure formed during polymer degradation around particle agglomerates. In the third stage (after t_2), the roughness increased slowly, probably due to a

very slight change in topographical structure. It might be related to the shielding effect of the densely and uniformly distributed P$_A$ nanoparticles on the surface. For latex − P$_C$ coating under the wet condition (indicated as dotted lines in Fig. 7a), the RMS roughness curve can also be divided into three stages. In the first stage (before t_1'), no obvious changes were observed, due to the erosion of the thicker clear layer. In the second stage (between t_1' and t_2'), the roughness increased slowly, due to the formation of some pits around the particle clusters. In the third stage (after t_2'), the roughness increased dramatically, due to growing and merging of the pits and the severe degradation around the large particle clusters.

Noticeably, the time frame for stage 1 was longer in AU − P$_C$ than in AU − P$_A$ under both the wet and dry conditions, due to a thicker clear layer observed in the AU − P$_C$ coating. For AU − P$_C$ coating under both wet and dry conditions, the slopes of the roughness curves increased much faster after the nanoparticle agglomerates appeared on polymer surface, as the severe localized degradation around large particle agglomerates contributed to the dramatic increase in surface roughness. However, the slopes of the roughness curves of AU − P$_C$ coatings did not reach the third stage of the AU − P$_A$ within the experimental range. It might be due to the different degradation processes in the two coatings, as evidenced by the different degradation patterns. The degradation of AU − P$_C$ coating was a very inhomogeneous process, attributed from the severe localized degradation around the poorly-dispersed particle agglomerates combined with slower degradation in unfilled polymer matrix. Whereas, the degradation of AU − P$_A$ coating was progressing around many uniformly distributed small
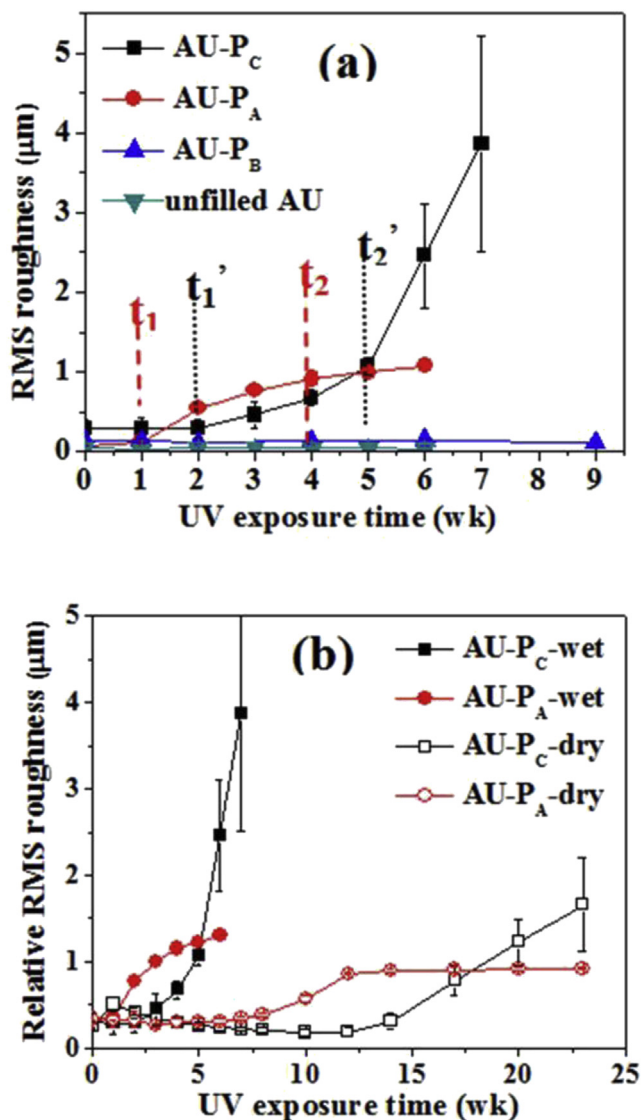
Fig. 7. (a) RMS surface roughness as a function of UV exposure time for unfilled AU, AU − P_A, AU − P_B, and AU − P_C coatings under the wet condition. (b) Relative surface roughness as a function of UV exposure time for AU − P_A and AU − P_C under the wet and dry conditions. For comparison, all curves were normalized to the initial roughness value of AU − P_C − wet at time zero. The error bar represented the standard deviation from the average of 4 measurement areas. The time lines t_1, t_2, t_1' and t_2' indicated different stages in the degradation processes, as described in the text.

agglomerates. Note that RMS data were obtained from averages of many large areas and the RMS surface roughness curve was closely correlated with the surface morphological changes. In summary, the surface roughness changes were not only well-correlated with the surface morphological changes, but more importantly, they also reflected the nanoparticle dispersion in the coatings.

4. Concluding remarks

In this study, the effect of heterogeneity of nanoparticle dispersion on the surface photodegradation was studied for the nano-TiO$_2$ filled AU coatings under both wet and dry conditions exposed with UV radiation. It was found that UV radiation is the primary and the most important factor in initiating photodegradation. Photoreactivity (or photocatalytic effect) of nanoparticles and humidity/moisture are as significant factors as

prodegradants in accelerating photodegradation. The dispersion of photoreactive nanoparticles dominates the surface photodegradation patterns and thereby significantly affects the degradation process of the polymer coatings.

Without UV radiation, nano-TiO$_2$ could not be photoexcited, and no chain scission would occur in polymer coatings, and thereby, photooxidation and photodegradation could not happen. Without higher relative humidity (moisture), the photodegradation would be slower, as fewer high reactive radicals would be formed to initiate the polymer degradation. Without higher photoreactive nanoparticles, the degradation would also be slower, as photostable TiO$_2$ could not be photoexcited by UV radiation to participate in the subsequent photooxidation. Provided with the aforementioned factors (UV radiation, moisture, photoreactivity), the effect of nanoparticle dispersion on degradation process could be demonstrated during the photodegradation. Based on the results in this study, the heterogeneity of the nanoparticle dispersion plays a significant role in affecting the degradation process and dominating the surface morphological evolution.

References

[1] Hussain F, Hojjati M, Okamoto M, Gorga RE. Polymer-matrix nanocomposites, processing, manufacturing, and application: an overview. J Compos Mater 2006;40:1511−75.

[2] Krishnamoorti R, Vaia RA. Polymer nanocomposites: synthesis, characterization, and modeling (ACS Symposium series). American Chemical Society; 2002.

[3] Aguirre M, Paulis M, Leiza JR. Particle nucleation and growth in seeded semibatch miniemulsion polymerization of hybrid CeO$_2$/acrylic latexes. Polymer 2014;55:752−61.

[4] Gu XH, Michaels C, Drzal P, Jasmin J, Martin D, Nguyen T, et al. Probing photodegradation beneath the surface: a depth profiling study of UV-degraded polymeric coatings with microchemical imaging and nano-indentation. J Coat Technol Res 2007;4:389−99.

[5] Forster AM, Watson SS, White J. Elastic modulus characterization of nano-composite latex coatings. In: Fernando RH, Sung LP, editors. Nanotechnology applications in coatings (ACS Symposium series). Oxford University Press; 2009. p. 274−90.

[6] Fukuda N, Tsuji H. Physical properties and enzymatic hydrolysis of poly(L-lactide)−TiO$_2$ composites. J Appl Polym Sci 2005;96:190−9.

[7] Chen XD, Wang Z, Liao ZF, Mai YL, Zhang MQ. Roles of anatase and rutile TiO$_2$ nanoparticles in photooxidation of polyurethane. Polym Test 2007;26:202−8.

[8] Chhabra V, Pillai V, Mishra BK, Morrone A, Shah DO. Synthesis, characterization, and properties of microemulsion-mediated nanophase TiO$_2$ particles. Langmuir 1995;11:3307−11.

[9] Sano T, Negishi N, Kutsuna S, Takeuchi K. Photocatalytic mineralization of vinyl chloride on TiO$_2$. J Mol Catal A-Chem 2001;168:233−40.

[10] Watson SS, Tseng IH, Forster A, Chin JW, Sung LP. Investigating pigment photoreactivity for coatings applications: methods development. In: Martin JW, Ryntz R, Chin JW, Dickie R, editors. Service life prediction for polymeric materials: global perspectives. Springer Press; 2008. p. 423−56.

[11] Watson SS, Tseng IH, Marray T, Pellegrin B, Comte J. Pigment and nanofiller photoreactivity database. J Coat Technol Res 2012;9:443−51.

[12] Ohno T, Sarukawa K, Tokieda K, Matsumura M. Morphology of a TiO$_2$ photocatalyst (Degussa, P-25) consisting of anatase and rutile crystalline phases. J Catal 2001;203:82−6.

[13] Clerici C, Gu XH, Sung LP, Forster AM, Ho DL, Stutzman P, et al. Effect of pigment dispersion on durability of a TiO$_2$ pigmented epoxy coating during outdoor exposure. In: Martin JW, Ryntz R, Chin JW, Dickie R, editors. Service life prediction for polymeric materials: global perspectives. Springer Press; 2008. p. 475−92.

[14] Wang D, Watson SS, Sung LP, Tseng IH, Bouis C, Fernando R. Effect of TiO$_2$ pigment type on the UV degradation of filled coatings. J Coat Technol Res 2011;8:19−33.

[15] Liu Z, Jin J, Chen S, Zhang J. Effect of crystal form and particle size of titanium dioxide on the photodegradation behavior of ethylene-vinyl acetate copolymer/low density polyethylene composite. Polym Degrad Stab 2011;96:43−50.

[16] Gesenhues U. Influence of titanium dioxide pigments on the photodegradation of poly(vinyl chloride). Polym Degrad Stab 2000;68:185−96.

[17] Allen NS, Edge M, Ortega A, Sandoval G, Liauw CM, Verran J, et al. Degradation and stabilisation of polymers and coatings: nano versus pigmentary titania particles. Polym Degrad Stab 2004;85:927−46.

[18] Chin JW, Byrd E, Embree N, Martin JW, Tate JD. Ultraviolet chambers based on integrating spheres for use in artificial weathering. J Coat Technol 2002;74:39−44.

[19] Chin JW, Nguyen T, Byrd E, Martin JW. Validation of the reciprocity law for coating photodegradation. J Coat Technol Res 2005;2:499−508.

[20] Kino GS, Corle TR. Confocal scanning optical microscopy and related imaging systems. Academic Press; 1996.

[21] Sung LP, Jasmin J, Gu X, Nguyen T, Martin JW. Use of laser scanning confocal microscopy for characterizing changes in film thickness and local surface morphology of UV exposed polymer coatings. J Coat Technol Res 2004;1: 267−76.

[22] Colling JH, Dunderdale J. The durability of paint films containing titanium dioxide − contraction, erosion and clear layer theories. Prog Org Coat 1981;9: 47−84.

[23] The NIH freeware ImageJ developed by National Institutes of Health (NIH), downloaded from http://rsb.info.nih.gov/ij/.

[24] Gu XH, Pang YY, Lin CC, Liu KP, Nguyen T, Chin JW. Linking accelerated laboratory and outdoor exposure results for PV polymeric materials − a mechanistic study of EVA. In: Dhere NG, Wohlgemuth JH, Lynn KW, editors. Reliability of photovoltaic cells, modules, components, and systems VI (Proceedings of SPIE)vol. 8825. SPIE-Int Soc Optical Engineering; 2013. 88250L-1−88250L-15.

[25] Therias S, Larché JF, Bussière PO, Gardette JL, Murariu M, Dubois P. Photochemical behavior of polylactide/ZnO nanocomposite films. Biomacromolecules 2012;13:3283−91.

[26] Miyazaki K, Arai T, Nakatani H. Polypropylene plasticization and photodegradation with a TiO_2/poly(ethylene oxide)/methyl linoleate paint photocatalyst system. J Appl Polym Sci 2014;131:39909-1−39909-8.

[27] Allen NS, Edge M, Corrales T, Childs A, Liauw CM, Catalina F, et al. Ageing and stabilisation of filled polymers: an overview. Polym Degrad Stab 1998;61: 183−99.

[28] Takeshita Y, Becker E, Sakata S, Miwa T, Sawada T. States of water absorbed in water-borne urethane/epoxy coatings. Polymer 2014;55:2505−13.

[29] Copinet A, Bertrand C, Govindin S, Coma V, Couturier Y. Effects of ultraviolet light (315 nm), temperature and relative humidity on the degradation of polylactic acid plastic films. Chemosphere 2004;55:763−73.

[30] Yang XF, Tallman DE, Bierwagen GP, Croll SG, Rohlik S. Blistering and degradation of polyurethane coatings under different accelerated weathering tests. Polym Degrad Stab 2002;77:103−9.

[31] Gerlock JL, Smith CA, Cooper VA, Dubiber TG, Weber WH. On the use of fourier transform infrared spectroscopy and ultraviolet spectroscopy to assess the weathering performance of isolated clearcoats from different chemical families. Polym Degrad Stab 1998;62:225−34.

[32] Nguyen T, Martin JW, Byrd E, Embree N. Relating laboratory and outdoor exposures of coatings: II. Effects of relative humidity on photodegradation and the apparent quantum yield of acrylic melamine. J Coat Tech 2002;74: 65−80.